AIP | Applied Physics Letters

Non-spectroscopic surface plasmon sensor with a tunable sensitivity

Qiuling Wen, Xu Han, Chuang Hu, and Jiasen Zhang

Citation: Applied Physics Letters **106**, 031113 (2015); doi: 10.1063/1.4906453
View online: http://dx.doi.org/10.1063/1.4906453
View Table of Contents: http://scitation.aip.org/content/aip/journal/apl/106/3?ver=pdfcov
Published by the AIP Publishing

Non-spectroscopic surface plasmon sensor with a tunable sensitivity

Qiuling Wen,[1] Xu Han,[1] Chuang Hu,[1] and Jiasen Zhang[1,2,a)]
[1]*State Key Laboratory for Mesoscopic Physics and Department of Physics, Peking University, Beijing 100871, China*
[2]*Collaborative Innovation Center of Quantum Matter, Beijing 100871, China*

(Received 7 December 2014; accepted 12 January 2015; published online 21 January 2015)

We demonstrate a non-spectroscopic surface plasmon sensor with a tunable sensitivity which is based on the relationship between the wave number of surface plasmon polaritons (SPPs) on metal film and the refractive index of the specimen in contact with the metal film. A change in the wave number of the SPPs results in a variation in the propagation angle of the leakage radiation of the SPPs. A reference light is used to interfere with the leakage radiation, and the refractive index of the specimen can be obtained by measuring the period of the interference fringes. The sensitivity of the sensor can be tuned by changing the incident direction of the reference light and this cannot be realized by conventional surface plasmon sensors. For a reference angle of 1.007°, the sensitivity and resolution of the sensor are 4629 μm/RIU (RIU stands for refractive index unit) and 3.6×10^{-4} RIU, respectively. In addition, the sensor only needs a monochromatic light source, which simplifies the measurement setup and reduces the cost. © *2015 AIP Publishing LLC*.
[http://dx.doi.org/10.1063/1.4906453]

Surface plasmon polaritons (SPPs) are surface waves confined to and propagating along a metal-dielectric interface.[1] The propagation constant of SPPs is extremely sensitive to even a slight change in the refractive index of specimen contacting the metal film. Utilizing this unique characteristic, surface plasmon resonance (SPR) sensors have been extensively studied in the past two decades as a powerful optical technique for label-free detection of biomolecules.[2,3] The SPR sensors are based on different detection methods such as measuring extinction spectra of gold nanorods,[4] scattering spectra of single silver nanocubes,[5] reflection spectra of gold nanopyramids,[6] transmission spectra of a fiber with bimetallic film or silver nanogratings or gold nanohole arrays,[7–10] interference spectra between two SPP waves[11,12] or between the SPP waves and the incident field,[13–17] angular spectrum of reflected light,[18,19] and measuring interference pattern generated by the SPP waves and the incident field.[20,21] However, the sensitivities of these surface plasmon sensors are unchangeable for a fixed metal structure, which cannot be conveniently used for the detection of refractive index change of different specimens, such as gases, vapors, liquids, or mixed solutions.[22]

Here, we experimentally demonstrate a plasmonic refractive index sensor based on the fact that the refractive index of the specimen over a metal film determines the propagation direction of the leakage radiation of the SPPs at the interface between the specimen and the metal film. By measuring the period of interference fringes generated by the leakage radiation and a reference light, the refractive index of the specimen can be obtained. The sensor we proposed has a tunable sensitivity with a fixed metal structure. Here, a relatively well established leakage radiation microscopy (LRM) system[23–26] was used and the transverse length of the detection area can be small, which is suitable for microfluidic chips. In addition, the respective control of the intensities of the leakage radiation and the reference beam results in high-contrast interference fringes.

The experiment setup is schematically depicted in Fig. 1(a). A 50-nm-thick gold film is thermally evaporated onto a cover glass. A grating is imprinted into the gold surface using a focused ion beam (FIB) milling system, and the top view of a scanning electron microscopy (SEM) image of the grating is shown in Fig. 1(b), which has five grooves. The period of the grating is the same as the wavelength of the SPPs λ_{SPP} at the interface between the gold film and pure water. In the experiment, the specimen is NaCl-H_2O solutions of different concentrations.

A laser beam with a wavelength of $\lambda_0 = 830$ nm is focused along the direction of the grating grooves by a cylindrical lens and then normally incidents onto the grating to excite SPPs, the launched SPPs propagate along the interface

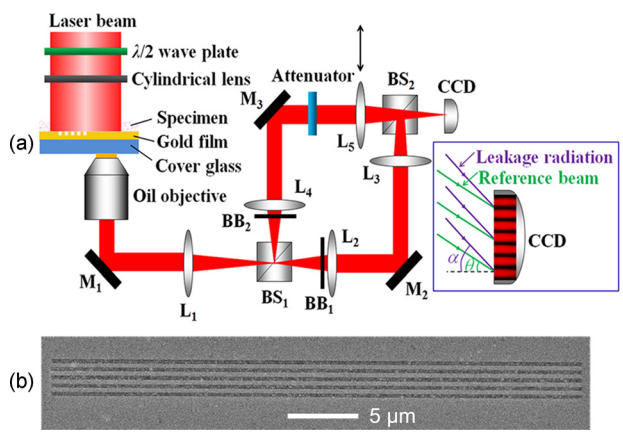

FIG. 1. (a) Schematic of the experimental setup. The inset shows the working mechanism of interference between the leakage radiation of SPPs and the reference beam. (b) SEM image of a SPP launching grating with 5 grooves.

a)Electronic mail: jszhang@pku.edu.cn

between the gold film and the specimen. Since the thickness of the gold film is 50 nm, a part of incident light can transmit directly through the gold film, which acts as the reference beam. Meanwhile, if the real part of the effective refractive index $\mathrm{Re}[n_{\mathrm{eff}}]$ of the propagating SPPs at the specimen/gold interface is smaller than the refractive index of the glass substrate n_s, the SPPs can radiate into the glass substrate, and the emission angle of the leakage radiation depends on $\mathrm{Re}[n_{\mathrm{eff}}]$.[23] The leakage radiation interferes with the reference beam and the interference fringes are measured by a home-built LRM system. The intensity profile of the SPPs is imaged onto a charge coupled device (CCD) (Basler scA780-54 gm, 782×582 resolution, 8.3 μm pixel size) camera using an oil-immersion objective (100×, NA = 1.4), two mirrors, M_1 and M_2, three lenses, L_1, L_2, and L_3 with identical focal lengths of 120 mm, and two beam splitters, BS_1 and BS_2. A beam block (BB_1) is used in front of L_2 to spatially block the directly transmitted laser light.[24] In the reference arm, the directly transmitted laser beam is imaged onto the CCD camera using the objective, two mirrors, M_1 and M_3, three lenses, L_1, L_4, and L_5 with identical focal lengths of 120 mm, and BS_1 and BS_2. The leakage radiation of the SPPs in the reference arm is filtered out using a beam block BB_2 in front of L_4.[24] Here, the position of L_5 can be moved along the direction of the black arrow indicated in Fig. 1(a) so as to vary the incident angle of the reference beam.[23] The leakage radiation and the reference beam interfere on the CCD camera and the interference fringes are obtained. An attenuator is used to control the intensity of the reference light in order to obtain high-contrast interference fringes. The inset in Fig. 1(a) depicts a schematic diagram of interference between the leakage radiation of the SPPs and the reference beam on the CCD camera. The angle between the reference beam and the normal line of the CCD is defined as θ, which can be adjusted by moving the position of L_5. The angle between the propagation direction of the leakage radiation and the normal line of the CCD is denoted by α, which depends on the refractive index of the specimen.

In the experiment, the normally incident beam and the launched SPPs interfere at the gold film/specimen interface, and the period of the interference fringes is equal to λ_{SPP}. Because λ_{SPP} depends on the dielectric environment in contact with the metal, the fringe period, as well as the propagation angle of the leakage radiation of the SPPs, would change with the variation of the refractive index of the dielectric adjacent to the metal layer. Both the reference beam and the leakage radiation of the SPPs are imaged onto the CCD camera with the LRM system. When the two beams encounter on the CCD plane, the interference fringes are generated and the corresponding interference intensity on the CCD camera can be written as

$$I = |E_{\mathrm{R}}|^2 + |E_{\mathrm{LR}}|^2 + 2|E_{\mathrm{LR}}||E_{\mathrm{R}}| \cos\left[(k_0 \sin\alpha - k_0 \sin\theta) \cdot x + \varphi_0\right], \quad (1)$$

where E_{R} and E_{LR} are the electric field amplitudes of the reference light and the leakage radiation, respectively. k_0 is the wave number of the incident light and φ_0 is the initial phase difference. The period of the interference fringes can be derived as $T = \lambda_0/|\sin\alpha - \sin\theta|$. In the case of normal incidence of the reference beam ($\theta = 0°$), the corresponding fringe period $T_0 = \lambda_0/\sin\alpha = M\lambda_{\mathrm{SPP}}$, where λ_0 is the wavelength of the incident light and M is the amplification factor of the LRM system. For the experiment setup here, M equals 72.2. The value of M is obtained by dividing the grating length on the CCD plane by the grating length on the gold film surface. Since $\sin\alpha = \lambda_0/M\lambda_{\mathrm{SPP}} = \mathrm{Re}[n_{\mathrm{eff}}]/M$, where $\mathrm{Re}[n_{\mathrm{eff}}] = \lambda_0/\lambda_{\mathrm{SPP}}$ and its value can be obtained by solving the specimen/50-nm-thick gold film/glass waveguide. Substituting $\sin\alpha = \mathrm{Re}\,[n_{\mathrm{eff}}]/M$ into $T = \lambda_0/|\sin\alpha - \sin\theta|$, the period of the interference fringes can be expressed as

$$T = \lambda_0/|\mathrm{Re}[n_{\mathrm{eff}}]/M - \sin\theta|. \quad (2)$$

For a large range of the refractive index of the specimen, the relationship of $\mathrm{Re}[n_{\mathrm{eff}}]$ and the refractive index of the specimen n_{d} is shown in Fig. 2. Here, n_{d} ranges from 1.0 to 1.34 and the $\mathrm{Re}[n_{\mathrm{eff}}]$ ranges from 1.0198 to 1.3936. As can be seen, $\mathrm{Re}[n_{\mathrm{eff}}]$ varies linearly with n_{d} in a large range. The red line in Fig. 2 represents a linear fit to the numerical points (black circles) and the corresponding mathematical expression is $\mathrm{Re}[n_{\mathrm{eff}}] = 1.0898n_{\mathrm{d}} - 0.07$. Hence, Eq. (2) can be written as

$$T = \lambda_0/|(1.0898n_{\mathrm{d}} - 0.07)/M - \sin\theta|. \quad (3)$$

It is obvious that the period of the interference fringes T depends on the reference angle θ and the refractive index of specimen n_{d}. Using Eq. (3), the periods of the interference fringes versus the refractive indices of specimen for $\theta = 1.2°$ (black line) and 2.2° (blue line) are depicted in Fig. 3. Here, the values of α range from 0.809° to 1.106° with respect to n_{d} ranging from 1.0 to 1.34. It is seen that the black curve in Fig. 3 has a nonlinear shape for the reference angle $\theta = 1.2°$, which is very close to the maximal value of leakage radiation angle ($\alpha = 1.106°$), and the blue curve is linear for a large range of n_{d} when the reference angle $\theta = 2.2°$. For the nonlinear case, the sensor can still be used for sensing because the refractive index of the specimen can be obtained from the nonlinear fit of the measured fringe period using Eq. (3).

Utilizing Eq. (3), the variation of the period of the interference fringes dT with respect to the change of the refractive index of the specimen dn_{d} can be written as $dT = 1.0898T^2/(M\lambda_0) \times dn_{\mathrm{d}}$. Thus, the sensitivity of the sensor which is defined as $S = dT/dn_{\mathrm{d}}$ can be written as

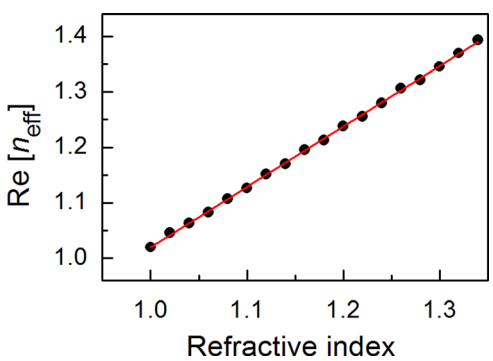

FIG. 2. Real part of effective refractive index of the leakage radiation of the SPPs versus the refractive index of the specimen.

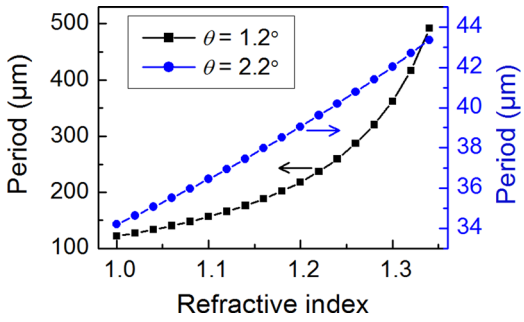

FIG. 3. Periods of the interference fringes versus refractive indices of specimen for reference angles θ equal 1.2° and 2.2°.

$S = 1.0898T^2/(M\lambda_0)$. It is apparent that a larger period means a higher sensitivity. To evaluate the intrinsic detection limits of the proposed sensor, we use a figure of merit (FOM) to characterize the sensing quality, which is defined as the sensitivity S divided by half of the fringe period T, similar to that in Ref. 20. Hence, the theoretical FOM can be expressed as $\text{FOM} = S/(T/2) = 2.18\,T/(\text{M}\lambda_0)$.

In the experiment, the concentrations of NaCl-H_2O solutions are 0%, 1%, 2%, 3%, 4%, and 5% (mass%) and the corresponding refractive indices of NaCl-H_2O solutions with different concentrations are 1.3216, 1.3233, 1.3250, 1.3267, 1.3285, and 1.3302, which were measured using the same method as in Ref. 11. The corresponding values of the leakage radiation angles α are 1.0875°, 1.0890°, 1.0904°, 1.0919°, and 1.0949°, obtained from $\alpha = \arcsin[(1.0898n_d - 0.07)/M]$. Using Eq. (3), we can obtain the periods of interference fringes for different reference angles as a function of the refractive indices of NaCl-H_2O solutions, as depicted in Fig. 4. The red lines represent the least-squares fitting to the numerical points (black circles). It is seen that the relationship between the periods of the interference fringes and the refractive indices of specimen exhibits good linearity for n_d with a small variation range of 0.0086. The sensitivity of the sensor can be derived from the slope of the fitting line in Fig. 4. The linear fits give the sensitivities of 1126, 2064, 4953, and 24394 μm/RIU (refractive index unit) for reference angles being 0.9°, 0.95°, 1°, and 1.05°, respectively. The

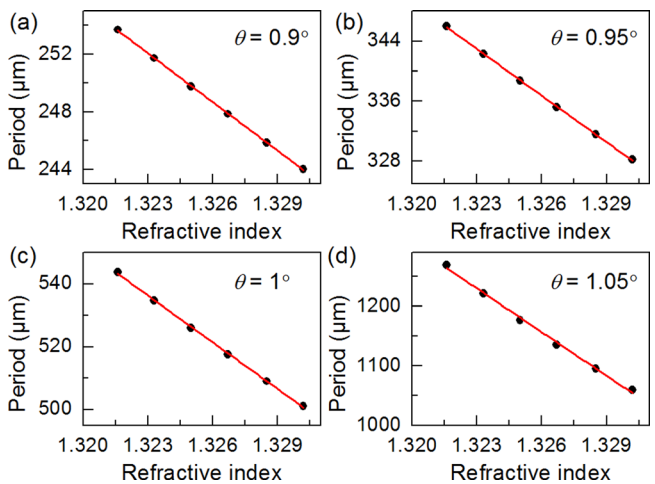

FIG. 4. Periods of the interference fringes for different reference angles θ versus refractive indices of NaCl-H_2O solutions with different concentrations.

corresponding FOMs are 9, 12, 19, and 41 RIU^{-1}. It is obvious that the closer the leakage radiation angle α to the reference angle θ, the higher the sensitivity and the larger the FOM. However, the number of pixels used to record the interference fringes is limited. A larger period results in a smaller number of periods, which degrades the measurement accuracy of the period. As a trade-off, the angle of the reference beam θ was set to be around 1° in the experiment. If the specimen is mixed vapor, a sensitivity of 4953 μm/RIU can be obtained for the reference angle θ being 0.72°.

When the 2% NaCl-H_2O solution was used as the specimen, the images of the reference beam and the leakage radiation are shown in Figs. 5(a) and 5(b), respectively, and their interference fringes are shown in Fig. 5(c). The position of the image of the grating is indicated by two vertical dashed lines in Figs. 5(a) and 5(c). The black curve in Fig. 5(d) is the intensity profile of the interference fringes along the horizontal dashed line in Fig. 5(c). The fringe period is obtained by fitting the intensity profile between the two vertical lines in Fig. 5(d) with a sine function (the red curve). Here, the fringe period is 569 μm on the CCD detection plane and the corresponding reference angle $\theta = 1.007°$, which is obtained from Eq. (3).

In order to characterize the sensing performance of the proposed sensor, we used NaCl-H_2O solutions of different concentrations (0%, 1%, 2%, 3%, 4%, and 5%) as the

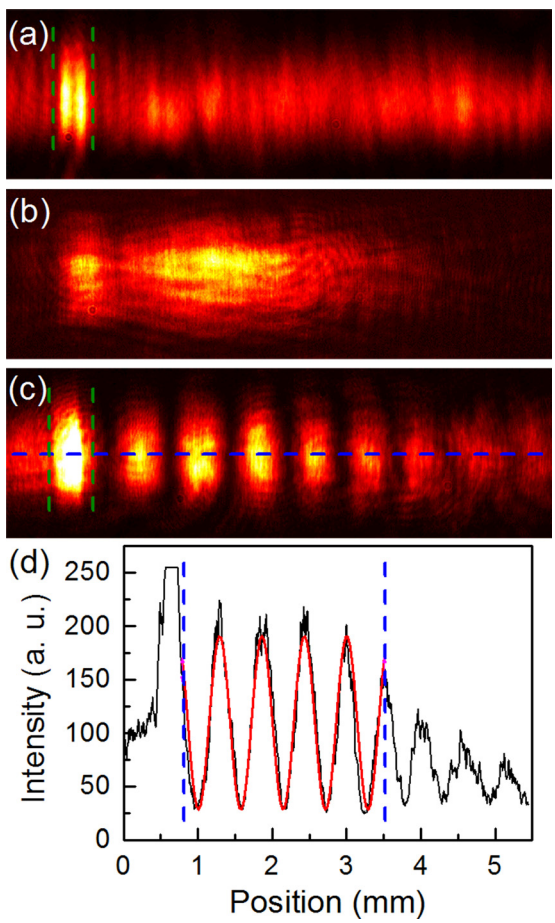

FIG. 5. Images of (a) the reference light, (b) the leakage radiation, and (c) the interference pattern. (d) Intensity profile of the interference fringes along the horizontal line in (c). The red curve is the sine fitting of the experimental data between the two vertical blue lines.

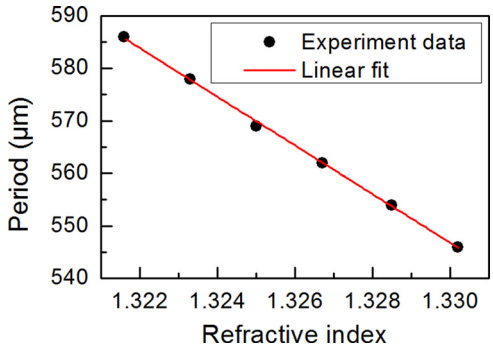

FIG. 6. Periods of the interference fringes versus refractive indices of NaCl-H_2O solutions with different concentrations.

specimen. The corresponding periods of the interference fringes given by the sine fitting are 586, 578, 569, 562, 554, and 546 μm, respectively, for $\theta = 1.007°$. Figure 6 shows the experimental results of the periods with respect to the refractive indices of the NaCl-H_2O solutions of different concentrations for $\theta = 1.007°$. It is seen that the relationship between the periods of the interference fringes and the refractive indices is linear. The solid line in Fig. 6 represents a linear fit to the measured data. The sensitivity of the sensor is 4629 μm/RIU, which is derived from the slope of the fitting line in Fig. 6. The corresponding FOM is around 16 RIU^{-1}. Since the number of periods used for sine fitting is five [Fig. 5(c)] and the minimum detectable shift of the interference fringes is one pixel (8.3 μm), the detection resolution is $8.3\,\mu\text{m}/[5 \times 4629\ (\mu\text{m/RIU})] = 3.6 \times 10^{-4}$ RIU for $\theta = 1.007°$. The typical sensitivity and detection resolution of the proposed sensor are analogous to those in Refs. 20 and 21.

In summary, we have demonstrated a non-spectroscopic plasmonic refractive index sensor with a tunable sensitivity. The refractive index of the specimen on a thin metal film can be obtained by measuring the period of the interference fringes between the leakage radiation of SPPs and a reference light. The sensitivity of the sensor is tunable for a fixed metal structure, which makes it can obtain a high sensitivity in different specimens. Moreover, the proposed sensor only needs a monochromatic light, such as a diode laser. These characteristics make the sensor can be used in many important areas including medicine, environmental monitoring, biotechnology, drug, and food monitoring.

This work was supported by the National Natural Science Foundation of China under Grant No. 61377050 and the Research Fund for the Doctoral Program of Higher Education under Grant No. 20130001110050.

[1]H. Raether, *Surface Plasmons on Smooth and Rough Surfaces and on Gratings* (Springer, New York, 1988).
[2]J. Homola, S. S. Yee, and G. Gauglitz, Sens. Actuators, B **54**, 3 (1999).
[3]K. M. Mayer and J. H. Hafner, Chem. Rev. **111**, 3828 (2011).
[4]K. M. Mayer, S. Lee, H. Liao, B. C. Rostro, A. Fuentes, P. T. Scully, C. L. Nehl, and J. H. Hafner, ACS Nano **2**, 687 (2008).
[5]L. J. Sherry, S.-H. Chang, G. C. Schatz, R. P. Van Duyne, B. J. Wiley, and Y. Xia, Nano Lett. **5**, 2034 (2005).
[6]P.-Y. Chung, T.-H. Lin, G. Schultz, C. Batich, and P. Jiang, Appl. Phys. Lett. **96**, 261108 (2010).
[7]A. K. Sharma and B. D. Gupta, Nanotechnology **17**, 124 (2006).
[8]B. Zeng, Y. Gao, and F. J. Bartoli, Appl. Phys. Lett. **105**, 161106 (2014).
[9]A. Barik, L. M. Otto, D. Yoo, J. Jose, T. W. Johnson, and S.-H. Oh, Nano Lett. **14**, 2006 (2014).
[10]A. E. Cetin, A. F. Coskun, B. C. Galarreta, M. Huang, D. Herman, A. Ozcan, and H. Altug, Light: Sci. Appl. **3**, e122 (2014).
[11]X. Wu, J. Zhang, J. Chen, C. Zhao, and Q. Gong, Opt. Lett. **34**, 392 (2009).
[12]Y. Gao, Q. Gan, Z. Xin, X. Cheng, and F. J. Bartoli, ACS Nano **5**, 9836 (2011).
[13]J. Feng, V. S. Siu, A. Roelke, V. Mehta, S. Y. Rhieu, G. T. R. Palmore, and D. Pacifici, Nano Lett. **12**, 602 (2012).
[14]Y. Gao, Z. Xin, B. Zeng, Q. Gan, X. Cheng, and F. J. Bartoli, Lab Chip **13**, 4755 (2013).
[15]T. Bian, B.-Z. Dong, and Y. Zhang, Plasmonics **8**, 741 (2013).
[16]V. S. Siu, J. Feng, P. W. Flanigan, G. T. R. Palmore, and D. Pacifici, Nanophotonics **3**, 125 (2014).
[17]B. Zeng, Y. Gao, and F. J. Bartoli, Nanoscale **7**, 166 (2015).
[18]J. Guo, P. D. Keathley, and J. T. Hastings, Opt. Lett. **33**, 512 (2008).
[19]A. K. Sharma and R. Jha, J. Appl. Phys. **106**, 103101 (2009).
[20]X. Li, Q. Tan, B. Bai, and G. Jin, Opt. Express **19**, 20691 (2011).
[21]O. Yavas and C. Kocabas, Opt. Lett. **37**, 3396 (2012).
[22]K. Li, X. Ma, Z. Zhang, J. Song, Y. Xu, and G. Song, J. Phys. D: Appl. Phys. **47**, 405101 (2014).
[23]A. Bouhelier and G. P. Wiederrecht, Opt. Lett. **30**, 884 (2005).
[24]A. Drezet, A. Hohenau, A. L. Stepanov, H. Ditlbacher, B. Steinberger, N. Galler, F. R. Aussenegg, A. Leitner, and J. R. Krenn, Appl. Phys. Lett. **89**, 091117 (2006).
[25]J. Grandidier, S. Massenot, G. C. des Francs, A. Bouhelier, J.-C. Weeber, L. Markey, A. Dereux, J. Renger, M. U. Gonzalez, and R. Quidant, Phys. Rev. B **78**, 245419 (2008).
[26]J. Wang, J. Zhang, X. Wu, H. Luo, and Q. Gong, Appl. Phys. Lett. **94**, 081116 (2009).